Control of a Leading-Edge Flap using the Nose Pressure Distribution

M. L. Eglington*

ABSTRACT

The problem of controlling the deflection of a leading-edge flap has been investigated from an aerodynamic point of view. The effect of a leading-edge flap on a symmetrical Joukowski aerofoil (12% thickness-chord ratio) is investigated experimentally through a set of wind-tunnel tests and, to a limited extent, theoretically. This initial study shows that it may be possible to control the deflection of the flap, to prevent separation and optimize the C_l/C_d ratio, using the static pressure difference between symmetrical tappings at equal small surface distances from the leading edge, but on opposite surfaces of the aerofoil. In the process a linear relationship between this pressure difference and the angle of attack is obtained. Thus, a linear relationship between this pressure difference and C_1 is also obtained.

Nomenclature

α	angle of attack, relative to the original chord line
α_{ideal}	abscissa axis intercept of ΔC_p-vs-α curves
a	C_l-*vs*-α curve slope for finite-span wing
a_{2D}	C_l-*vs*-α curve slope for 2 dimensional (infinite-span) wing
AR	aspect ratio
b	constant in Joukowski transformation formula [mm]
β	angle determining camber of Joukowski aerofoil, 0° for aerofoils used
c	aerofoil chord length [mm]
C_d	drag coefficient
C_l	lift coefficient
C_p	pressure coefficient
ΔC_p	difference in C_p between pressure tappings at equal surface distances from the original leading edge, but on opposite surface of the aerofoil
e	fractional horizontal eccentricity of the circle centre for Joukowski transformation
ρ	density [kg/m³]
S	aerofoil surface area [m²]
s	aerofoil span [mm]
U	free stream velocity [m/s]

Introduction

The Function and Effect of a Leading-Edge Flap

Modern-fighter-aircraft aerofoils are designed for optimum performance at high subsonic and transonic speeds, this dictates a thin aerofoil with very little camber and a sharp leading edge, otherwise the drag coefficient and shockwave effects at high Mach numbers are excessive. The problem with such an aerofoil is that it is prone to separation, and thus lift failure, at high angles of attack. The result is two-fold; first, the maximum lift coefficient is limited and thus the low-speed (take-off and landing) performance is poor. Second, the manouvrability in 'dog-fight' situations is limited. A leading-edge flap is a high-lift device, which improves the aerofoil's performance under these conditions by permitting higher angles of attack.

Figure 1 shows how a leading-edge flap decreases the severity of the corner through which the flow must turn in order to remain attached at high angles of attack. Thus, the acceleration and expansion of the flow around the upper surface of the leading edge and the corresponding lift generating suction pressures are more evenly distributed along the upper surface. The aerofoil is therefore able to reach a higher angle of attack before the negative (gauge) pressure becomes low enough to cause reversal

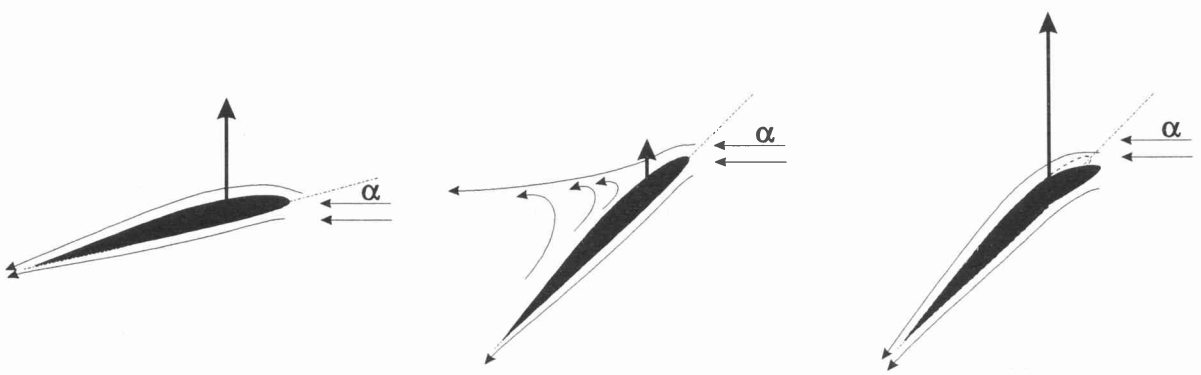

a) At low angle af attack, flow stays attached and aerofoil produces lift.

b) At high angle of attack, separation causes loss of lift.

c) Effect of leading-edge flap is to prevent separation at high angle of attack.

Figure 1 – Effect of a leading-edge flap

* Final year Mechanical Engineering student 1991, University of Natal

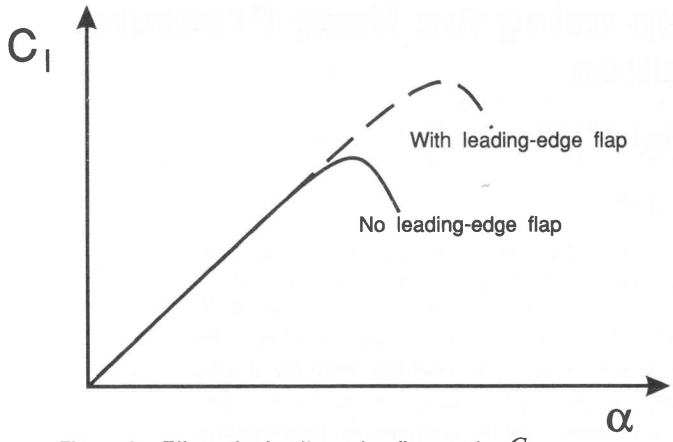

Figure 2 – Effect of a leading-edge flap on the C_l-vs-α curve

and separation of the upper-surface flow. The effect of a leading-edge flap on a typical lift-coefficient (C_l) vs angle-of-attack (α) curve is shown in figure 2. Curve A represents the clean aerofoil (with no high-lift devices). Initially, while the flow is still attached, C_l increases linearly with angle of attack. As the angle of attack increases separation begins to occur causing the lift produced to decrease. The C_l-vs-α curve reaches a maximum when the lift-decreasing effect of increasing separation equals the lift-increasing effect of the increasing angle of attack; thereafter the lift drops rapidly with increasing α. By increasing the high-angle-of-attack capacity of the aerofoil, the leading-edge flap allows it to produce a higher maximum lift coefficient (curve B).

Control of a Leading-Edge Flap and the Scope of this Article

Due to the performance improvement described above, leading-edge flaps are now fairly common on modern fighter aircraft (for example the American F-18 and F-16). There are, however, a significant number of older aircraft whose performance could be notably improved by the addition of leading-edge flaps, for example the Mirage III.

One of the major problems that needs to be overcome in implementing leading-edge flaps, as an upgrade on older aircraft, is the control of deflection of the flaps. In a dog-fight situation in particular, the deployment must be automatic in response to the pilot's actions. Although there is very little literature available on the control of leading-edge flaps (in fact the author did not have access to any such information), modern aircraft employing leading-edge flaps are generally 'fly-by-wire' aircraft ie. sophisticated on-board computer and electronic equipment provides the interaction between the pilot and the control surfaces of the aircraft. It appears that existing leading-edge-flap control systems are an integrated part of these computer systems and use complicated algorithms, test data and air flight measurements to determine the flap deflection required by the pilot's actions. In any event computerised control is not a viable option for an upgrade because the aircraft in question do not have the required on-board computer systems and fitting of such systems is limited by cost and space considerations.

Therefore there is a need for a cheap, simple and easy-to-implement method of determining and controlling leading-edge-flap deflection. This is an investigation into a possible solution ie. to try to correlate the static-pressure distribution on the nose section of the leading-edge flap with the performance characteristics of the aerofoil under varying angles of attack and flight speeds for different flap deflections. The aim is to obtain a simple relationship which could be used to realise a feedback control system which would control the flap deflection so as to prevent separation and optimize performance using static-pressure tappings from the nose of the wing as a feedback variable.

Outline of Procedure

The effect of a leading-edge flap on a symmetrical Joukowski aerofoil of 12% thickness-to-chord ratio with a chord length of 280mm was investigated by building and testing the following three aerofoils:
aerofoil 1: symmetrical Joukowski aerofoil.
aerofoil 2: symmetrical Joukowski with leading 20% rotated through 7,5°.
aerofoil 3: symmetrical Joukowski with leading 20% rotated through 15°.

The aerofoil profiles are shown in figure 3. The static-pressure distributions, lift and drag coefficients, and separation characteristics of these profiles were investigated experimentally and, to a limited extent, theoretically at varying angles of attack and flow speeds. The experimental results were analysed for a correlation between the lift, drag and separation characteristics and the pressure distribution.

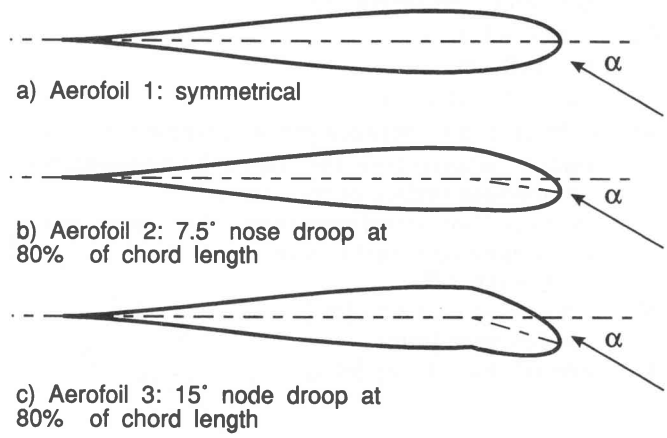

Figure 3 – Aerofoil profiles

Theoretical Investigation

The Kutta-Joukowski transformation is a well-known conformal transformation which transforms a circle into an aerofoil shape. The equations for the transformation of a circle into an aerofoil of given thickness-to-chord ratio and chamber are developed and described in, inter alia, Houghton and Brock [1]. Joukowski aerofoils were used because, although the aerofoil produced is a not practically useful one, it is easy to predict the inviscid flow around it using Potential-Flow Theory and conformal-transformation theory. Using these theories Houghton and Brock develop equations for the lift and pressure coefficients in terms of the geometry and angle of attack, α, of the aerofoil. Thus simple equations for the theoreti-

cal static-pressure distribution and lift coefficient of the symmetrical aerofoil were obtained.

The effect of the leading-edge flap on the lift and pressure coefficients was analyzed using thin-aerofoil theory as described by [1] and Kuethe and Schetzer [2].

Limitations of the Theory

Complete theoretical modelling of a wing in viscous flow is a complex problem and the theories mentioned above have several idealizations and limitations:

Assumption of Inviscid Flow

The theories described assume that the fluid (air in this case) has zero viscosity. Thus they do not account for the effects of the viscous boundary layer and provide no estimate for the viscous drag.

(i) Effect on Pressure and Lift

For attached flow around an aerofoil the pressures and lift predicted by inviscid theories should be accurate because the effects of viscosity are limited to the (thin) viscous boundary layer.

(ii) Effect on Drag

In general there are two main types of drag on aerofoils:

- *profile drag*, which is independent of lift and includes surface-friction drag and form drag. Surface-friction drag is the drag resulting from the viscous shear stresses between the fluid and the aerofoil surface and cannot exist in inviscid flow. Form drag is due to the component of the resultant pressure force in the stream (drag) direction. For inviscid flow it can be shown that this component is always zero.
- *induced drag*, on the other hand, is lift dependent and caused by trailing-edge vortices, which are initiated by the pressure-equalizing flow from the pressure surface to the suction surface at the tips of a finite-length aerofoil. It can be shown ([1] for example) that drag can indeed exist in inviscid flow and is roughly dependent on the square of the lift coefficient giving the $C_l$vs-C_d curve its characteristic quadratic shape.

Thus inviscid theories do not provide useful estimations of the drag on an aerofoil in viscous flow, and it was beyond the scope of the project to attempt accurate theoretical modelling of the drag on the aerofoils.

(iii) Effect on Separation

Separation is a viscous phenomenon and cannot occur in inviscid flow. Therefore the theories above provide no information on the separation characteristics of the aerofoils.

Singularities in the Thin-Aerofoil Theory

Thin-aerofoil theory involves replacing the airofoil by a vortex sheet, which creates an overall lift producing circulation, a velocity distribution and thus a pressure distribution along itself. This pressure distribution can be integrated to find the lift force. The vortex sheet representation, however, predicts infinite velocities at the leading and trailing edges. Thus the theory is singular at these points. The singularity at the trailing edge can be eliminated by forcing the Kutta condition and the singularity at the leading edge is integrable; thus the lift predicted by the integration of the vorticity distribution is reliable.

But, because the pressure is dependent on the velocity, the theoretical pressure distribution is particularly inaccurate near the leading edge. In fact, for round-nosed aerofoils in particular, the theory should predict a stagnation point at or near the leading edge (to conform with reality), which it does not. Thus the nose-pressure distribution predicted by thin-aerofoil theory is not useful for comparison with experiment.

The theory can, however, be made uniformly valid using singular perturbation theory. This theory is developed in detail by Van Dyke [4]; chp. 4 in particular deals with 'Singular Perturbation Problems in Thin Airfoil Theory.' Here Van Dyke develops Lighthill's rule: a multiplicative correction factor for the velocity, which renders thin-aerofoil theory uniformly valid near round aerofoil edges.

In essence, Lighthill's rule corresponds to fitting an osculating parabola centred on the expected stagnation point on the round edge. An exact potential-flow solution for the velocity on a parabola is available, and, according to Van Dyke, a uniformly-valid solution for the thin-aerofoil problem may be obtained by multiplying the velocity predicted by thin-aerofoil theory, by a correction factor equal to the ratio of the exact solution for the parabola, to the thin-aerofoil solution for the region near to the nose. The reasoning is that 'near the leading edge, where the disturbances are large, the exact speed on the airofoil is nearly that on the osculating parabola. Far from the edge, on the other hand, the correction factor approaches unity, so that the thin-airfoil solution is recovered where it is valid'. (Van Dyke 1975: p.60). Although time restraints prevented the extension of this analysis to a quantitative stage, the principles described above will be used later to explain some of the results obtained.

Effect of Low Aspect Ratio and Large Size of the Aerofoils Relative to the Test Section

The theories discussed so far are strictly only true for two dimensional aerofoils (ie. having infinite span), in infinite uniform flow fields. The experimental set-up differed from this ideal in several ways:

(i) The aerofoils were tested in an open-section wind tunnel with an outlet height of only 2.5 times the chord length. (Note that this large chord length was necessary in order to obtain acceptable accuracy in the lift, drag, and pressure distribution measurements.) This means that the aerofoils will be deflecting only a narrow stream of air (as opposed to an infinite stream) and thus the force required to change the momentum of the stream and deflect it will be lower. Therefore the lift force and pressures generated by the aerofoil will be lower than predicted by two dimensional theory.

(ii) The edges of the aerofoils extended a little (7% of span) beyond the edges of the jet of flow and the aerofoils had a low aspect ratio:

$$AR = \frac{s^2}{S} = 1{,}18. \qquad (1)$$

The important effect here is again that the experimen-

tal pressures and resulting lift coefficients will be significantly lower than those predicted by the two-dimensional theories. This is due to the pressure-equalizing flow to and from the adjacent undisturbed atmospheric air at the edges of the jet of flow over the aerofoils. Due to the low aspect ratio, these edge effects will affect a relatively large portion of the entire flow; they will therefore cause a significant overall reduction of the pressures and lift generated by the aerofoils.

Concluding Comments
Due to the limitations of the theory and the complexity of complete and accurate modelling of a 3 dimensional wing in viscous flow, the spirit of this project was to look for correlation between the trends indicated by the specific theories above (and by other theory and experiment in the literature) and the actual experimental results, rather than to aim for accurate numerical agreement. The usefulness of the theoretical investigation was thus rather to provide confidence in the experimental results by indicating that the aerofoils were exhibiting reasonable known behaviour.

Experimental Details

Construction of the Aerofoils
General Design

As shown in figure 4, each aerofoil was constructed from six 50 mm long wooden segments, which were assembled on mild steel aligning rods to give a span of 300 mm. The aerofoils had a chord length of approximately 255 mm and a designed thickness-to-chord ratio of 12%. To facilitate measurement of the static pressure at the surface, span-wise holes were drilled through the full span. During testing these holes were blocked at one end and connected to a manometer at the other. Small 0,5 mm holes, cross drilled from the surface into these span-wise holes, enabled the surface pressure distribution to be measured.

Generation of Profiles
A Turbo Pascal 5.0 computer program was written to generate the points for the Joukowski profiles using the standard Kutta-Joukowski transformation described by [1]. Sufficient profile points were generated to obtain a smooth profile ie. double point density on the nose section, and a Lagrangian-cubic-polynomial interpolation was used to maintain the smooth profile at the discontinuities caused by the rotation of the nose section.

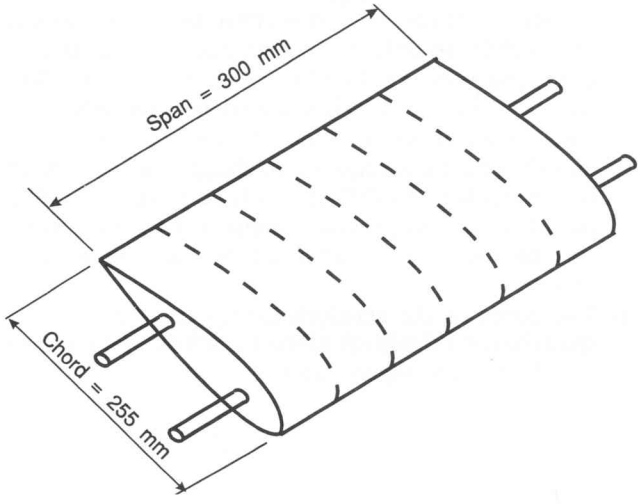

Figure 4 – General design of the aerofoils

Machining of the Aerofoils
The aerofoils were end-milled from blocks of jelutong and imbuia on a Maho 600 CNC milling machine by simply linearly interpolating between the profile points, while traversing in a clockwise direction around the profile; hence the highpoint density required on the nose section. The spanwise pressure-tapping holes and the spanwise aligning holes in each segment were also drilled with the CNC machine before the segment was removed.

Assembly and Accuracy of the Aerofoils
The Maho milling machine had an accuracy of 0.001 mm, but this obviously cannot be achieved with wood. Also, during assembly of the aerofoils, a minimal amount of sanding was required to smooth the aerofoils in the spanwise direction, owing to inaccuracies caused by wandering of the thin drill bit when drilling the wood. The profiles were thus accurate to about $\pm$ 1 mm. Another inaccuracy was caused by the cusped trailing edges of the Joukowski profiles; they were too thin and broke off during machining. As a result the aerofoils had chord lengths of approximately 255 mm as opposed to the designed 280 mm. This change in chord length should have minimal effect on the lift and pressure because the pressure coefficients near the trailing edge are close to zero anyway.

Sealing of Aerofoils and Pressure-Tapping Holes
A fairly major problem encountered was the leaking of the pressure-tapping holes, owing to the porosity of the wood and small gaps at the joints between the segments of the aerofoils. Such leaking is unacceptable because it leads to inaccurate measurement of the static pressure due to flow in the pressure measuring tubes. The problem was overcome by spray-painting the aerofoils with Glatex 8 polyurethane paint to seal the outer surface. Interaction between the span-wise pressure holes was prevented by injecting Glatex 8 through them with a hypodermic syringe. Short lengths of aluminium tubing were forced into the span-wise holes in each aerofoil, when the paint was still wet, to facilitate connection to the manometer. All the holes were then satisfactorily leak and plug tested, and the aerofoils were lightly sanded to obtain a smooth surface ready for testing.

Experimental Procedure:

General Outline
The aerofoils were tested in the Department's open-section recirculating low-speed wind tunnel. Lift and drag were measured with a mechanical 3-component wind-tunnel balance, pressures were measured with a multi-tube manometer, and the flow speed was measured with a pitot-static tube. The tests were carried out over several weeks at standard atmospheric conditions in Durban. The atmospheric pressure during testing ranged from

752.5-754.0 mmHg and the average room temperature was 25°C.

Size of Test Section and Positioning of Aerofoils
The tunnel outlet at the test section was 260 mm wide and 650 mm high. The aerofoils were mounted on the tunnel centre-line, such that, at zero angle of attack, the leading edge was 40 mm from the plane of the outlet. Since the aerofoils had a span of 300 mm and were mounted symmetrically with respect to the tunnel centre-line, the edges of the aerofoils extended 20 mm past the edge of the jet on each side. The velocity distribution was investigated with the pitot-static tube and a traverse gear: near the outlet the velocity varied as a steep step function, which became progressively more rounded further from the outlet, but was still constant over the major portion of the trailing egde of the aerofoil.

Test Speeds and Reynolds Numbers
The aerofoils were tested at 4 speeds as shown in table 1 below and at angles of attack increasing from zero to separation in increments of 2°.

Table 1: Test Speeds and Reynolds Numbers

	[m/s]	[km/hr]	Reynolds No.
Speed 1	22.45	80.52	3.64×10^5
Speed 2	30.19	108.7	4.89×10^5
Speed 3	38.33	138.0	6.21×10^5
Speed 4	44.54	160.3	7.22×10^5

The Reynolds numbers in table 1 are based on true chord length of 255 mm.

Experimental and Theoretical Results

As expected, after being non-dimensionalized with the dynamic pressure ($\frac{1}{2}\rho U^2$), the results at each of the four different speeds were similar. For this reason, the results included below are mainly for speed 3 ie. 38.33 m/s, $Re = 6.21 \times 10^5$.

C_l-vs-α Curves
The experimental lift-coefficient vs angle-of-attack curves are shown superimposed on the same axes in figure 5.

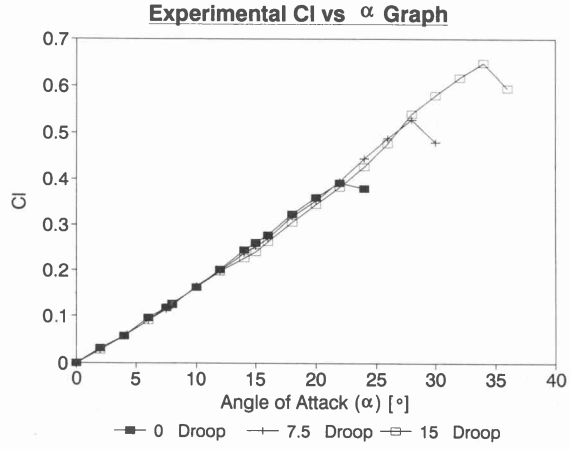

Figure 5 – Experimental C_l-vs-α curves

(i) As expected, the effect of the leading-edge flap is to delay the onset of separation, allowing the aerofoil to handle a higher angle of attack and produce a higher maximum lift coefficient. Table 2 compares the angles of attack at which separation occurred and the corresponding maximum lift coefficients.

Table 2: Occurrence of Separation (speed = 38 m/s)

Aerofoil	Flap Deflection	α at Separation	C_l at Separation
1	0°	22°	0,34
2	7.5°	28°	0,53
3	15°	34°	0,65

(ii) Particularly noticeable is the similarity of the three curves: they have the same slope, lie almost on top of each other, and pass through the origin. This means that neither the slope, nor the zero-lift angle of attack **(relative to the original chord line)** was affected by drooping the nose. It is not intuitively obvious that drooping the nose should scarcely affect the zero-lift angle of attack, but this result is supported by the thin-aerofoil calculations in (iii) below, and in fact Kuethe and Schetzer [2] prove (with thin-aerofoil theory) that the effect of a change in the camber line near the trailing edge, on the zero-lift angle of attack, is far greater than the effect of a change near the leading edge.

(iii) Houghton and Brock [1] show that the theoretical lift coefficient for a 2-dimensional Joukowski aerofoil in inviscid flow is

$$C_l = 2\pi(1 + e)\sin(\alpha + \beta.) \qquad (2)$$

Substituting the values of the transformation constants used to obtain a 12% thickness-to-chord ratio, symmetrical aerofoil (ie. $e = 0.092379$, $\beta = 0$) gives

$$C_l = 2{,}18\pi\sin\alpha. \qquad (3)$$

Differentiation of w.r.t. α *gives the ideal inviscid two-dimensional C_l-vs-α slope for aerofoil 1:*

$$\frac{\partial C_l}{\partial \alpha} = 2{,}18\pi\cos\alpha. \qquad (4)$$

For small α this will be approximately constant and equal to 2π per radian, and according to [1] it is 'well established that all conventional aerofoils in low speed conditions, that is conditions in which compressibility effects can be largely ignored, have [constant] two-dimensional lift slopes of between 6 and 5,5 per radian.'

Using thin-aerofoil theory, it can be shown [1] that the lift coefficient of the flapped aerofoils is given by an expression of the form

$$C_l = 2\pi A_0 + \pi A_1, \quad (5)$$

where A_0 is a term dependent on the angle of attack and the mean-camber-line shape, and A_1 is a constant dependent on the mean-camber-line shape of the aerofoil. For the symmetrical aerofoil, it can be shown that $A_0 = \alpha$ and that $A_1 = 0$ so that

$$C_{l_0} = 2\pi\alpha. \quad (6)$$

Similar equations for the flapped aerofoils can be obtained using the known geometry of the flapped aerofoils to calculate A_0 and A_1. They are

$$C_{l_{7,5^\circ}} = 2\pi\alpha - 0.03396 \quad (7)$$
$$C_{l_{15^\circ}} = 2\pi\alpha - 0.06625 \quad (8)$$

for the 7.5° and 15° nose-droop aerofoils respectively.

Note that in these equations α is relative to the original chord lines (as always in this article) and must be expressed in radians. Setting $C_l = 0$ in (7) and (8) and solving for the zero-lift angle of attack gives $\alpha_0 = 0.00540$ and 0.0105 radian (or 0.310° and 0.604°) for the 7.5° and 15° droop aerofoils respectively. Thus the theory predicts a small shift of the C_l-vs-α curves relative to each other, but no change in the slope. This trend agrees well with the experimental results in figure 5, especially since it is unlikely that the experimental set-up was accurate enough to pick up the small shifts in angle of attack.

(iv) It was also asserted above that the theoretical two-dimensional C_l-vs-α slope for each aerofoil is approximately 2π per radian. In sharp contrast to this is the experimental value of 1.10 per radian (from figure 5). In other words, the aerofoils produced significantly lower lift coefficients than predicted by theory. A probable explanation for this discrepancy is the combination of large chord length relative to the flow stream, low aspect ratio, and edge effects discussed earlier.

C_l-vs-C_d Curves

The experimental C_l-vs-C_d curves are shown in figure 6. The most important points to be noted from these curves are:

(i) They exhibit the typical C_l-vs-C_d curve shape ie. a quadratic dependence of C_l on C_d, owing to the trailing-vortex drag, and a horizontal shift from the origin, owing to the lift-independent drag component.

(ii) Corresponding to the increased maximum C_l values is an increase in the corresponding C_d values. This point is further emphasized by a comparison of the maximum C_l/C_d ratios for the different nose droops: the C_l/C_d ratio is an indication of the efficiency of the aerofoil, and the maximum ratio is determined by the slope of a line from the origin and tangential to the C_l-vs-C_d curves, as shown in figure 6. Comparison of the slopes shows that the effect of flap deflection is to decrease the maximum C_l/C_d ratio. Thus the increased lifting capacity of the wing must be paid for with increased drag and decreased aerofoil 'efficiency'; this is the reason for variable geometry high lift devices: they are only deployed when needed.

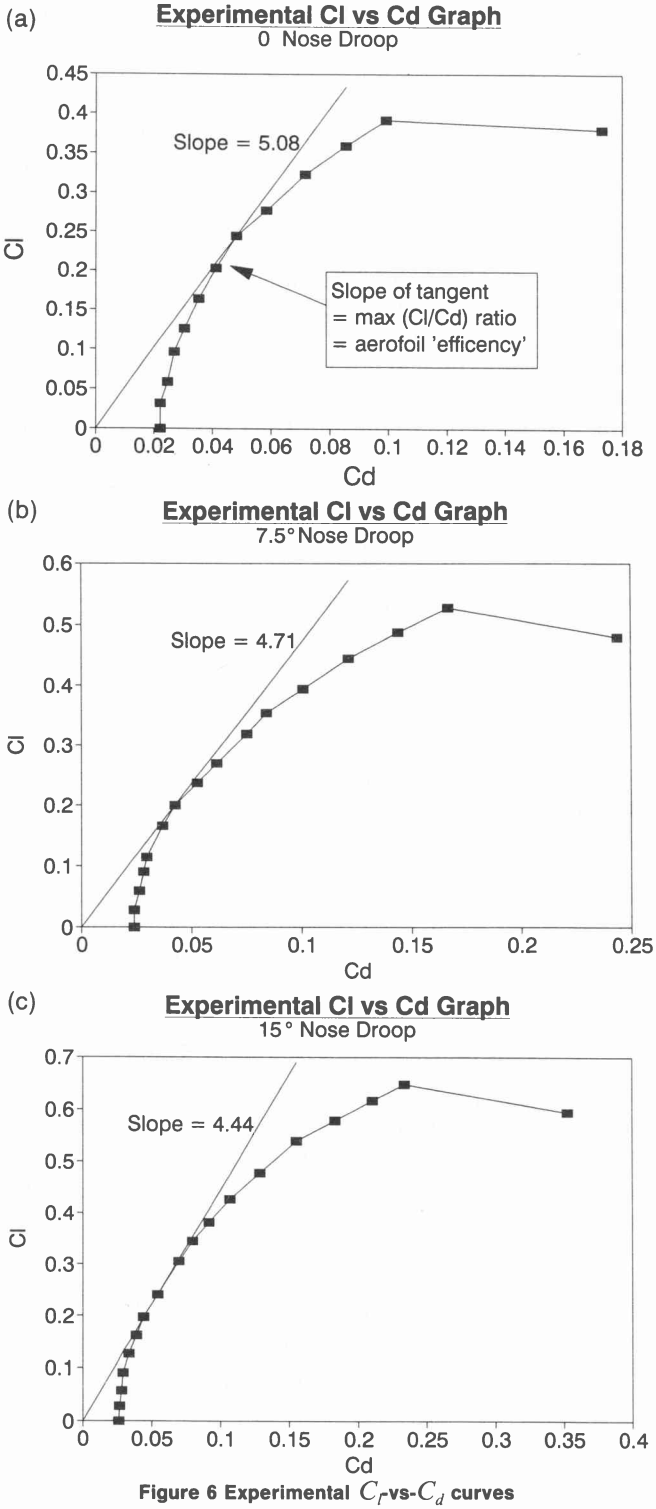

Figure 6 Experimental C_l-vs-C_d curves

ΔC_p vs α Curves

Here ΔC_p is the difference between the pressure coefficients at equal small distances from the (original) leading edge, but on the lower and upper surfaces of the aerofoil (as shown in figure 7) ie.

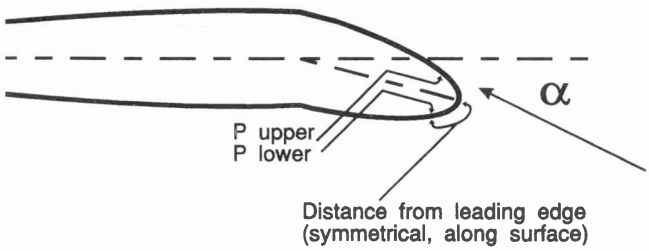

Figure 7 – ΔC_p tapping positions

$$\Delta C_p = C_{p_{pressure}} - C_{p_{suction}} = \frac{P_{lower} - P_{upper}}{\frac{1}{2}\rho U^2}. \quad (9)$$

ΔC_p values for several distances from the leading edge were calculated, both experimentally and theoretically (for the symmetrical foil only), and then plotted as functions of α. Note that these distances are measured along the aerofoil surface, not along the camber line.

The curves thus obtained were found to be remarkably linear, and therefore least-square-linear-regression lines were fitted to the data points. Typical experimental ΔC_p-vs-α curves (for distances 9 and 12 mm from the leading-edge), with least-square lines superimposed, are included in figure 8.

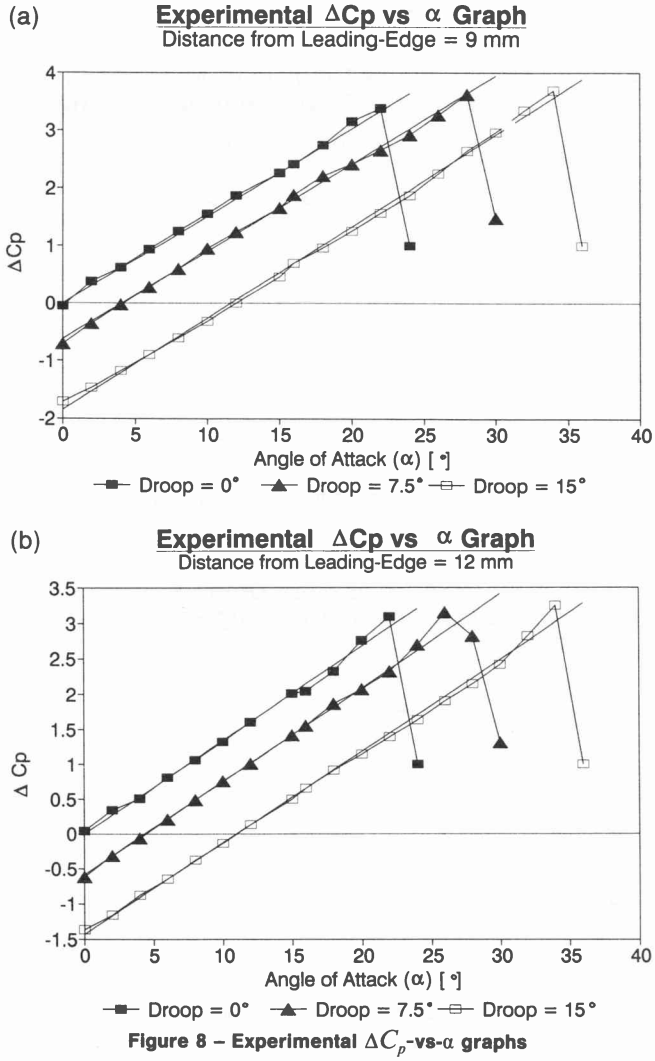

Figure 8 – Experimental ΔC_p-vs-α graphs

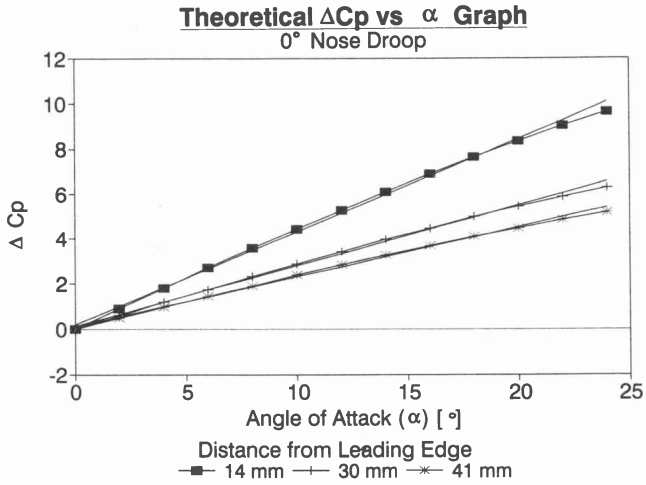

Figure 9 – Theoretical ΔC_p-vs-α lines

The experimental curves show that ΔC_p increases linearly with angle of attack until separation occurs (indicated by the sudden drop in ΔC_p). Particularly noticeable are the similar gradients for the 0°, 7.5° and 15° flap deflections, indicating that the constant of proportionality is independent of the flap deflection.

The second point to notice is that, just before separation occurs, ΔC_p reaches a critical value, $\Delta C_{p\,crit}$, which is approximately constant (allowing for experimental errors) and independent of the flap deflection.

Finally, it will be noted that the effect of flap deflection is only to horizontally shift the ΔC_p-vs-α line. This shift is indicated by the abscissa axis intercept α_{ideal} ie. the angle of attack at which $\Delta C_p = 0$. Increasing the flap deflection increases α_{ideal}.

As shown in figure 9, a relatively linear relationship was also obtained form the theoretical pressure distribution for the symmetrical aerofoil (obtained using the Joukowski Transformation and potential-flow theory as discussed by [1]). Unfortunately though, as mentioned, the potential-flow theories cannot predict separation characteristics, and time limitations prevented extension of quantitative theoretical predictions to the nose-drooped aerofoils. It will be noted that the values of ΔC_p predicted by the 2-dimensional analysis are significantly higher than those obtained experimentally, which is the reason why the theoretical results have not been superimposed on the experimental curves. Again this discrepancy is most likely due to the large chord length, low aspect ratio and edge effects discussed previously.

Effect of Distance from the Leading Edge

It is important to note that the results obtained here are most pronounced and usable for the tappings close to the leading edge. Figure 10, which shows the ΔC_p-vs-α graph for tappings 30 mm from the leading edge, illustrates this point.

The graphs in figure 11, below, further illustrate the effect of distance from the leading edge on the results. The first graph shows that although the gradient of the ΔC_p-vs-α lines decreases with distance from the leading edge, the gradients for the different flap deflections remain almost identical. The second graph plots the $\Delta C_{p\,crit}$ for each flap deflection vs distance form the leading edge.

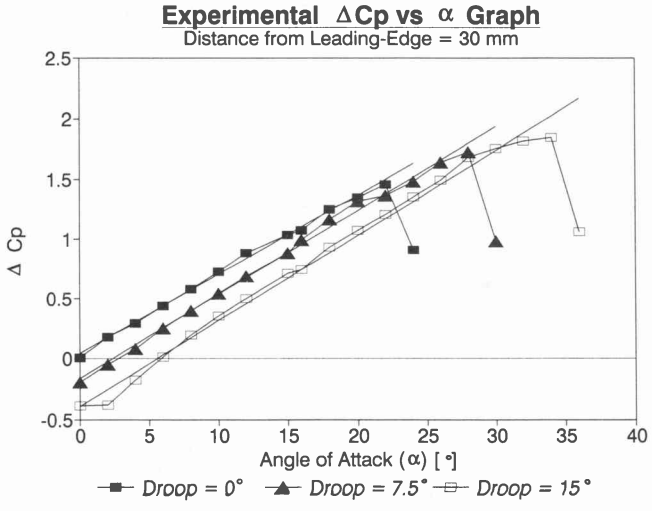

Figure 10 – Experimental ΔC_p-vs-α graph.

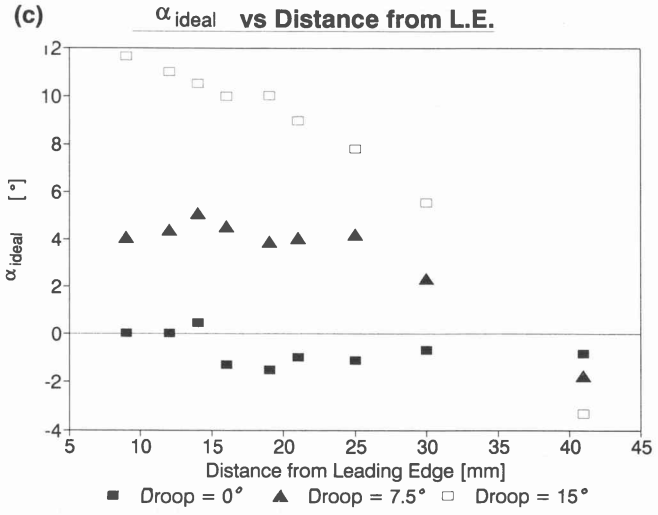

Figure 11 – Effect of distance from leading edge

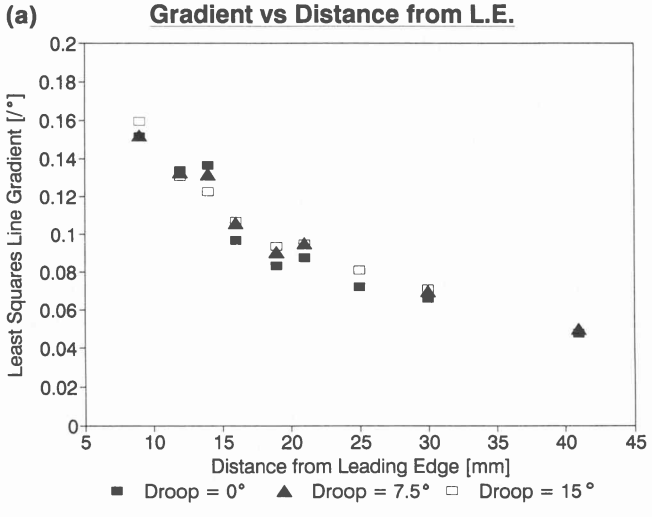

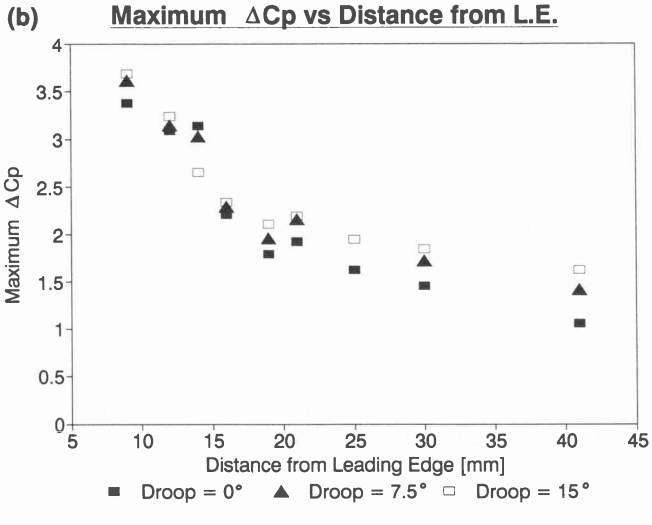

The general trend is for the deviation in $C_{p\ crit}$ to increase with distance from the leading edge. This may be more clearly seen by comparison of the ΔC_p-vs-α curves for distances 9, 12 and 30 mm from the leading edge, shown in figures 8 and 10. Finally, the plot of α_{ideal} vs distance from the leading edge shows that increments in α_{ideal} with flap deflection gradually decrease until, for tappings 41 mm from the leading edge, α_{ideal} decreases instead of increases with increasing flap deflection.

Effect of Speed

It was claimed earler that the experimental results were very similar at different speeds and Reynold's numbers; the comparative graphs in figure 12 illustrate this point.

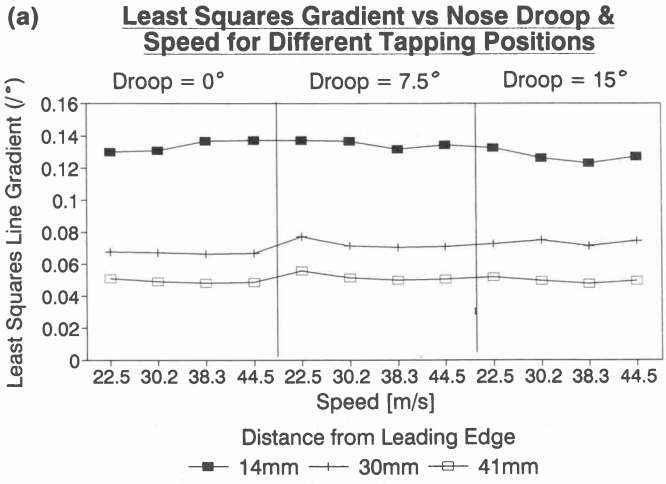

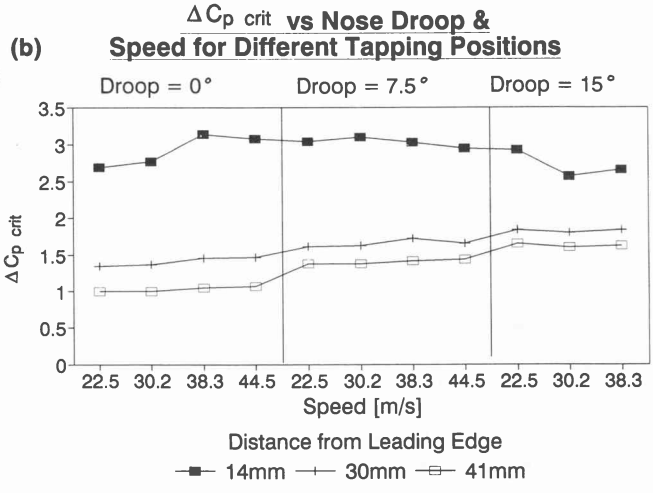

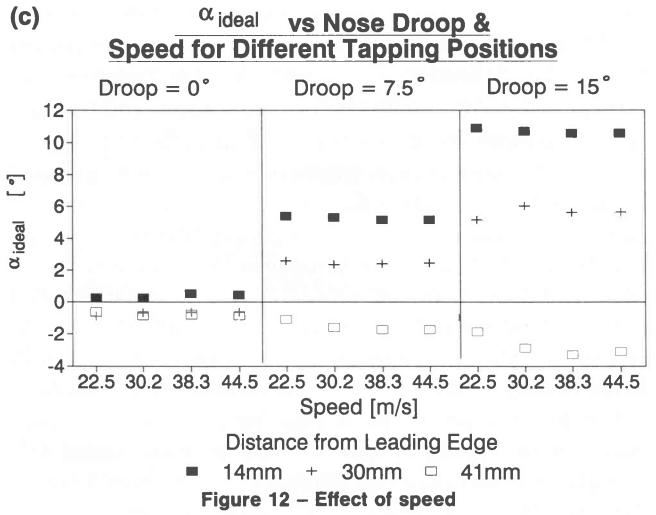

Figure 12 – Effect of speed

Summary of Most Useful Results

1. Effect of Leading-Edge Flap Deflection:
Deflecting the leading edge flap results in delayed separation and thus allows the aerofoil to produce a higher maximum lift coefficient C_l but this lift must be paid for in increased drag and decreased efficiency.

2. Investigation of ΔC_p vs Angle-of-Attack (α)

2.1 Within the attached flow regime, a linear relationship between ΔC_p and α was obtained ie.

$$\Delta C_p = k_1\alpha + constant. \tag{10}$$

Here k_1 was *independent* of flap deflection, *independent* of speed, but *dependent* on the tapping distance from the leading edge.

2.2 Just before separation occurs ΔC_p reaches a critical value, $\Delta C_{p\,crit}$, which is also *independent* of flap deflection and *independent* of speed, but *dependent* on the tapping distance from the leading edge.

2.3 The abscissa-axis intercept $-\alpha_{ideal}$ (ie. the angle of attack at which $\Delta C_p = 0$) is however, *dependent* on flap deflection while still being *independent* of speed and *dependent* on the tapping distance from the leading edge.

Significance for the Control of a Leading Edge Flap

The complete equation for the ΔC_p vs α lines is thus

$$\Delta C_p = k_1(\alpha - \alpha_{ideal}) < \Delta C_{p\,crit}. \tag{11}$$

The significance of these results for the problem of controlling the leading-edge flap are:

1. Separation may be avoided by keeping $\Delta C_p < \Delta C_{p\,crit}$.
2. ΔC_p can be reduced by increasing α_{ideal}; for tappings close enough to the leading-edge α_{ideal} can be increased by deflecting leading-edge flap. It follows that α_{ideal} is a measure of the high-angle-of-attack capability of the aerofoil: by deploying the leading-edge flap, α_{ideal} is increased and separation is delayed.
3. Once $\Delta C_{p\,crit}$ (for a specific aerofoil and tapping position) is determined, a feedback control system could be implemented to prevent separation by adjusting the flap deflection during flight to satisfy 1.
4. Since, in general, aerofoil 'efficiency', C_lC_d decreases with increasing camber (flap deflection), the control system may be optimized by minimizing flap deflection, while satisfying 1 (within a certain safety margin).
5. Finally, it has been shown that C_l is proportional to α:

$$C_l = k_2\alpha, \tag{12}$$

as is ΔC_p:

$$\Delta C_p = k_1(\alpha - \alpha_{ideal}) < \Delta C_{p\,crit}, \tag{13}$$

it follows, therefore, that $\Delta C_p \propto C_l$, and proportional determination of C_l for control purposes is possible. Solving for α in equation (13) and substituting in equation (12) gives

$$C_l = k_2\left(\frac{\Delta C_p}{k_1} + \alpha_{ideal}\right). \tag{14}$$

In order to implement such a control system, the values of k_1, k_2 and Delta $\Delta C_{p\,crit}$, as well as knowledge of the variation of α_{ideal} as a function of flap deflection for the given aerofoil and position of the pressure tappings will be required.

Physical Explanation
Consider the physical situation: the nose sections of each of the aerofoils are identical, except that they are rotated through an angle with respect to the trailing section. Therefore it seems intuitively likely that, close enough to the leading edge, the effects of the different trailing sections on the pressure distributions will be insignificant in comparison to the local effects of the nose shape. Thus one could expect that certain critical conditions, eg. the critical ΔC_p value, would prevail just before separation occurs at the nose, and that these would be approximately the same, independent of the leading-edge-flap deflection. One would also expect that these conditions would be shifted with respect to the angle of attack measured relative to the original chord line, ie. to depend rather on the effective angle of attack of the nose section. Thus the existence of a critical ΔC_p value, and the dependence of ΔC_p on α_{ideal} (which can be seen as an indication of the effective angle of attack) are physically understandable.

This idea is the essence of Van Dyke's derivation of Lighthill's correction formula for round edges in thin-aerofoil theory [4]. The basic principle is that, near enough to the leading edge, any round-nosed aerofoil will look very much like the nose of its osculating parabola, and thus will have a pressure distribution very similar to that of the parabola. Obviously Van Dyke gives a far more formal and in-depth analysis, but the point here is that the results are physically and theoretically understandable.

It is more difficult to explain the linearity of the ΔC_p-vs-α curve; it is best just to say that it follows from the above

reasoning that the gradient of these curves should be independent of the flap deflection.

Finally, it also follows from the physical reasoning, and from Van Dyke's theory, that the effects described should be more pronounced for pressure tappings closer to the leading edge.

Conclusion

In this project, the problem of controlling the deflection of a leading-edge flap has been investigated from the aerodynamic point of view. That is to pursue a relationship between the more easily measured aerodynamic characteristics of an aerofoil (pressure distribution in this case) and the inherently more difficult to measure characteristics (eg. lift, drag, and susceptibility to separation), which one wishes to control.

The effect of a leading-edge flap on an aerofoil's characteristics was explored by analyzing, both experimentally and theoretically, three aerofoils, based on a symmetrical Joukowski aerofoil of 12% thickness to chord ratio and chord length 280 mm, differing only by the angle through which the leading 20% of their profiles was drooped (0°, 7.5°, and 15°). Theoretically derived results from Potential-Flow theory and Thin-Aerofoil theory, as well as other theoretical and experimental results from the literature, were compared with the results of open-section wind-tunnel tests on the aerofoils. The experimental results were found to agree well with expected trends; in particular, typical C_l-vs-α (angle of attack) curves and C_l-vs-C_d curves were obtained experimentally.

Regarding the control problem, it was found that measurements of the static pressure difference, ΔC_p, between symmetrical points at equal small distances from the leading edge, but on opposite surfaces of the aerofoil, could be used as a feedback variable in a control system for the flap deflection: First, since ΔC_p reaches a certain critical value ($\Delta C_{p\ crit}$) just before separation, and because ΔC_p is reduced by increasing the flap deflection, separation of the wing at high angles of attack can be avoided by adjusting the flap deflection to keep $\Delta C_p < \Delta C_{p\ crit}$; this, as discussed, is the main function of the leading-edge flap. Secondly, because an aerofoil with increased camber (flap deflection) produces more drag than a less cambered aerofoil producing the same lift (cf. C_l/C_d ratios), this control system should minimize the flap deflection while still keeping $\Delta C_p < \Delta C_{p\ crit}$ (within a certain safety margin).

Finally, it must be noted that these results have only been shown experimentally for the aerofoils tested (although the linear ΔC_p-vs-α relationship was demonstrated theoretically for a symmetrical Joukowski aerofoil). Before this relationship can be implemented, the dependence of k_1, $\Delta C_{p\ crit}$ and α_{ideal} on the particular aerofoil shape and real three dimensional wing geometry must be investigated. This project is, however, a positive starting point. A possible topic for further investigation is to extend the quantitative predictions of the Thin-Aerofoil theory with Van Dyke's singular-perturbation methods [4].

Bibliography

1. Houghton, E. L. and Brock, A. E. 1970; *Aerodynamics for Engineering Students;* 2nd Ed., Arnold, London, 1970.

2. Kuethe, A. M. and Schetzer, J. D. 1959; *Foundations of Aerodynamics;* 2nd Ed., Wiley, New York, 1959.

3. Huenecke, K. 1987. *Modern Combat Aircraft Design;* 1st Ed., Airlife, England, 1987.

4. Van Dyke, M. 1975; *Perturbation Methods in Fluid Mechanics*; Annotated edition, The Parabolic Press, Stanford, California, 1975.